Molecular Therapy
Oncolytics
Original Article

In vivo DNA-launched bispecific T cell engager targeting IL-13Rα2 controls tumor growth in an animal model of glioblastoma multiforme

Pratik S. Bhojnagarwala,[1] Ryan P. O'Connell,[1] Daniel Park,[1] Kevin Liaw,[1] Ali R. Ali,[1] Devivasha Bordoloi,[1] Joel Cassel,[1] Nicholas J. Tursi,[1] Ebony Gary,[1] and David B. Weiner[1]

[1]Vaccine and Immunotherapy Center, The Wistar Institute, 3601 Spruce Street, Philadelphia, PA 19104, USA

Glioblastoma is an aggressive tumor with poor survival rates. Bispecific T cell engagers (BTEs) against different cancers are in various stages of clinical development. Toxicity resulting from cytokine release syndrome and the short half-life of BTEs, which necessitates continuous infusion, complicating delivery and increasing costs, are major challenges in the field. Here we describe the development of *in vivo* DNA-launched BTEs (dBTEs) with highly focused targeting of interleukin-13 receptor α2 (IL-13Rα2), a glioblastoma cell-surface target. We developed 4 BTEs targeting 2 epitopes of IL-13Rα2 and studied how heavy-light chain orientation affects BTE function. The dBTEs induced T cell activation, cytokine production, and tumor cytolysis in the presence of IL-13Rα2$^+$ tumor cells, but we observed unique patterns of immune activation. We found a strong correlation between granzyme B secretion and dBTE-induced cytolysis of specific and nonspecific tumors. We down-selected dBTE PB01-forward based on lower cytokine induction profile and highest activation specificity. *In vivo*, dBTE PB01-forward demonstrated an improved half-life versus intravenous recombinant BTE delivery. In an orthotopic glioblastoma model, dBTE PB01-forward controlled tumor growth, improving animal survival, supporting the hypothesis that the blood-brain barrier does not affect the function of systemically delivered dBTE. Further study of PB01-forward for targeting glioblastoma and other IL-13Rα2$^+$ cancers is warranted.

INTRODUCTION

Glioblastoma Multiforme (GBM) is a high-grade glioma representing the most common and aggressive form of malignant brain tumors.[1] Standard-of-care treatment for GBM involves surgery followed by radiation and chemotherapy.[2] Although these therapies provide short-term benefits,[3] GBM ultimately remains fatal. The median survival rate with current treatments is 15–16 months.[4] This indicates a substantial unmet and urgent need for improving therapeutic options for individuals with GBM.

Bispecific T cell engagers are bispecific antibodies comprised of two single-chain variable fragments (scFvs) that can simultaneously bind to two different antigens and bring them close to each other. Typically, one arm of the bispecific T cell engager (BTE) binds to a tumor-associated antigen (TAA), and the other end binds to the CD3 epsilon chain on T cells. Engagement of both arms of BTEs triggers T cell activation, leading to cytolysis of tumor cells. One such BTE targeting CD19 received US Food and Drug Administration (FDA) approval for treatment of acute lymphoblastic leukemia in 2014.[5] CD3-based bispecific antibodies can lead to cytokine release syndrome (CRS), which is a major clinical concern.[6] Additional challenges for current use of bispecific antibodies include manufacturing limitations and a short *in vivo* half-life, resulting in the need for continuous infusions over several weeks.[7] A delivery method resulting in longer *in vivo* expression could significantly improve the applicability of this technology.

We have previously described an approach of using synthetic DNA (synDNA)-encoded monoclonal antibodies for immunotherapy with improved expression kinetics.[6–8] This approach entails intramuscularly injecting a synDNA plasmid that encodes for the biologic agent into mice. This is followed by electroporation at the site of injection, which increases the transfection efficiency of the plasmid, resulting in more production in the muscle, which, in turn, results in improved secretion of bispecific antibody from the muscle into the serum. It is important to develop new T cell-redirecting therapies because of their exceptional potential for affected individuals; a simplified production scheme would improve the experience of treated persons while improving tumor control *in vivo*. In this regard, we have described the development of a DNA-launched HER2-targeting bispecific antibody that was expressed in mice for several weeks and showed impactful tumor control in an animal model of ovarian cancer.[8] Here we study this approach for targeting GBM. The interleukin-13 receptor α2 (IL-13Rα2) is a high-affinity receptor for IL-13 that likely acts as a decoy receptor because it contains a truncation resulting in a very short intracellular portion lacking signaling

Received 15 March 2022; accepted 3 July 2022;
https://doi.org/10.1016/j.omto.2022.07.003.

Correspondence: David B. Weiner, PhD, Vaccine and Immunotherapy Center, The Wistar Institute, 3601 Spruce Street, Philadelphia, PA 19104, USA.
E-mail: dweiner@wistar.org

capabilities.[9,10] There is increasing evidence that IL-13Rα2 is associated with a mesenchymal gene expression signature, more aggressive disease, and poor prognosis, suggesting that targeting this TAA would be costly to the tumor.[11] IL-13Rα2 is expressed on glioma-initiating cells, making it important for GBM tumors.[12] It is expressed on tumors of approximately 75% of individuals with GBM,[13,14] indicative of a high specificity for tumor tissue and minimal expression in other healthy tissue, making it an attractive target for GBM therapy.[15] Radiolabeled peptides targeting IL-13Rα2 have been shown to improve median survival in animal models of GBM.[16] Vaccination against peptides derived from IL-13Rα2 has been clinically effective in adults and children.[17,18] Finally, CAR T cells redirected against IL-13Rα2 have been described to target GBM tumors in animal models and are being studied in the clinic, so far with mixed results.[1,19–22] IL-13Rα2 is an important target for new immunotherapy approaches, including DNA-launched BTE (dBTE) therapy.

In this study, we developed a BTE against IL-13Rα2, which addresses several challenges associated with using BTEs for GBM. We initially designed 4 different BTEs based on 2 different scFvs targeting two different epitopes of IL-13Rα2. Targeting two different epitopes also allowed us to compare the efficacy and specificity of both antibodies. We further modified the orientation of the heavy and light chains encoding each scFv to identify an optimal arrangement that would yield high specificity and minimal off-target toxicity. These dBTEs were cloned into a high-expression mammalian plasmid vector and expressed *in vitro*. The V_L-V_H-V_H-V_L orientation is designated as the forward orientation, and the V_H-V_L-V_L-V_H orientation is designated as the reverse orientation. We compared T cell activation, cytokine secretion, and cytolysis capability of all BTEs to identify PB01-forward as a lead candidate. *In vivo*, we show that dBTEs had a better serum half-life and that peripherally delivered dBTEs controlled the growth of orthotopic GBM tumors. These results establish that the directionality of BTEs is an important consideration in the design phase of these novel therapeutic agents that can significantly affect the final functionality of the biologic agent. Fine-tuning the directionality of the BTE can result in improved tools for immunotherapy of this difficult-to-treat cancer.

RESULTS

dBTE design and expression

We identified two clones of IL-13Rα2 monoclonal antibodies from published studies of CAR T cells targeting IL-13Rα2.[19] The sequences were examined and redesigned for BTE expression cassettes. We selected sequences of the IL-13Rα2-targeting scFvs and included a glycine-serine linker to fuse them in frame to the scFv of a sequence encoding an optimized anti-CD3 antibody (modified from UCHT1)[8] to reconstruct a full dBTE. As described previously,[8] a novel leader sequence to allow better dBTE expression also facilitates secretion of product produced *in vivo*. We engineered all full constructs as new bispecific molecules for expression as DNA-encoded plasmids through DNA engineering and RNA and codon optimization. Because we were interested in the orientations of the construct designs, we generated modified orientations of the heavy and light chains of both scFvs, resulting in a total of 4 different dBTEs: two targeting one epitope of IL-13Rα2 and two targeting a different epitope. They were designated PB01-forward, PB01-reverse, PB02-forward, and PB02-reverse. The dBTEs in the V_L-V_H-V_H-V_L format are designated as the forward orientation, and those in the V_H-V_L-V_L-V_H format are designated as the reverse orientation (Figure 1A). We transfected Expi293F cells to study the 4 dBTEs from *in vitro* expression. The dBTEs were expressed at similar levels, as evidenced by detection in the transfection supernatants via western blots (Figure S1A). Both dBTEs in the forward orientation and those in the reverse orientation bound to CD3 on human T cells as well as to U87 cells expressing IL-13Rα2 (Figures 1B, 1C, S1B, and S1C). By binding ELISA, we confirmed that both dBTEs in forward and reverse orientation bound specifically to IL-13Rα2 but not to IL-13Rα1 (Figure 1D). We also evaluated the binding kinetics of the dBTEs by performing binding ELISAs using recombinant, purified versions of the BTEs. We also evaluated the binding characteristics of the BTEs to IL-13Rα2 using a surface plasmon resonance assay. Via both assays, we observed that all four BTEs bound to IL-13Rα2 with high affinity (Figures 1E and S2A). To characterize the binding of dBTEs to IL-13Rα2, we performed a competition ELISA. The data demonstrate that BTEs derived from the PB01 scFv did not affect binding of BTEs derived from the PB01 scFv to IL-13Rα2 and vice versa (Figure 1E). These data suggest that dBTEs derived from PB01 and PB02 bind to distinct epitopes of IL-13Rα2. Surprisingly, we observed significant differences in binding to recombinant CD3 protein, where we observed that the BTEs in the forward orientation had significantly lower affinity for CD3 compared with BTEs in the reverse orientation (Figure S2B).

dBTEs in the forward orientation specifically activate T cells in the presence of U87 cells *in vitro*

To test dBTE function, U87 cells and human T cells were co-cultured at an E:T ratio of 10:1 in the presence of the transfection supernatant. To test the effect of dBTE design (orientation of heavy and light chains) on the specificity of T cell activation, the T cells and dBTE were also cultured with ovcar3 cells, which do not express IL-13Rα2 (Figure S3). Using flow cytometry, T cell activation was measured based on expression of CD69 and PD-1 24 h and 48 h after co-culture.

We observed that, at each time point, in the presence of U87 cells, the dBTEs in the reverse orientation induced higher T cell activation compared with those in the forward orientation (Figures 2A, S4A, and S4B). Interestingly, we saw high levels of T cell activation induced by dBTEs in the reverse orientation even in the presence of ovcar3 cells. PB02-forward also induced $CD4^+$ T cell activation in the presence of ovcar3 cells. This was lower than that induced by dBTEs in the reverse orientation. PB01-forward only induced T cell activation in the presence of U87 cells, indicating a high degree of specificity for this dBTE. The data suggest that some non-specific or antigen-independent T cell activity is induced by the dBTEs in the reverse orientation, which could lead to potential non-specific toxicity *in vivo*.

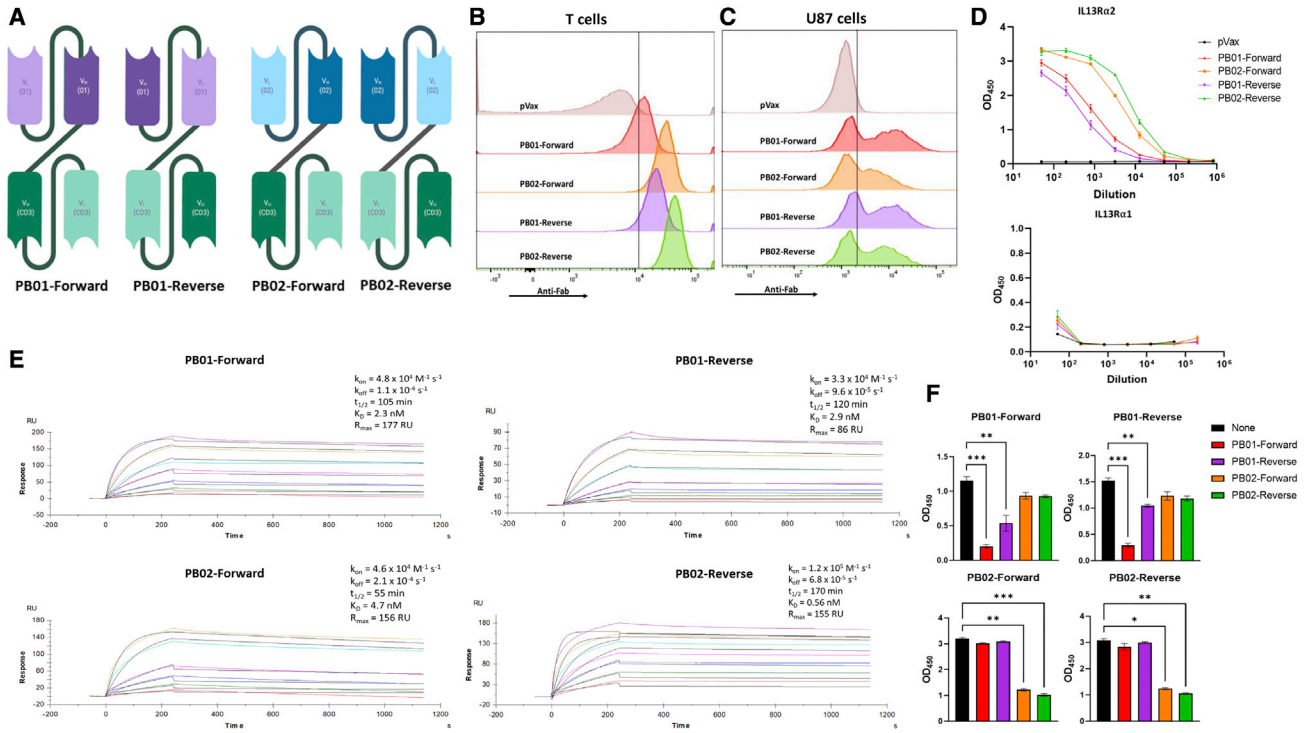

Figure 1. dBTE expression and binding to the target

(A) Design of 4 different dBTEs targeting IL-13Rα2. (B and C) Histogram plots showing binding of dBTEs to CD3 on primary human T cells and IL-13Rα2 on U87 cells, respectively. (D) Binding ELISA showing binding of all 4 dBTEs specifically to IL-13Rα2. (E) SPR data showing binding kinetics of all BTEs to recombinant IL-13Rα2. (F) Competition ELISA demonstrating that dBTEs derived from PB01 and PB02 bind to distinct epitopes of IL-13Rα2.

To characterize the different T cell responses induced by dBTEs in the forward orientation compared with those in the reverse orientation, we analyzed the cytokine profile in supernatants collected at 24 h of co-culture from the previous experiment. We found that all dBTEs increased the amount of Th1 cytokines, such as interferon (IFN)-γ, IL-2, and tumor necrosis factor alpha (TNF-α), and Th2 cytokines, such as IL-4, IL-6, and IL-10, in the presence of U87 cells (Figure 2B). In the presence of U87 cells, the levels of cytokine secretion induced by dBTEs was higher than that induced by dBTEs in the forward orientation. We also observed secretion of diverse cytotoxic granules (sFasL, perforin, granzyme A, and granzyme B) by T cells activated by dBTEs in the presence of U87 tumor cells (Figure 2C). Although dBTEs in the reverse orientation induced higher levels of most cytotoxic molecules in the presence of U87 cells, there was no significant difference in the levels of granzyme B across all four dBTEs. Similar to the flow cytometry-based assays, dBTEs in the reverse orientation elicited higher levels of some cytokines and cytotoxic molecules compared with dBTEs in the forward orientation in the presence of ovcar3 cells.

We observed low-level non-specific or antigen-independent secretion of cytokines with PB02-forward dBTE, especially IFN-γ, IL-6, and perforin. However, we observed the least expression of cytokines or cytotoxic molecule secretion from T cells when cultured with PB01-forward and ovcar3 cells.

dBTEs drive killing of target-expressing tumors *in vitro* in the presence of T cells

To follow tumor killing, we transfected U87 cells with GFP and firefly luciferase to create the U87-GFP-luc line. We co-cultured U87-GFP-luc cells with individual dBTEs and T cells at the indicated E:T ratios. Fluorescence images taken 48 h after co-culture showed a significantly reduced GFP signal in U87-GFP-luc cells co-cultured with all four dBTEs compared with those co-cultured with supernatant from pVax-transfected cells. We observed clustering of T cells around GFP^+ tumor cells in the presence of supernatant from dBTE-transfected cells. T cells in wells containing pVax supernatant were spread randomly over the wells, indicating that clustering of T cells around the target cells is dependent on the presence of dBTEs (Figure S5). The dBTEs also showed dose- and time-dependent lysis of U87-GFP-luc cells. There were no significant differences in toxicity across the four dBTEs (Figure 3A). To further characterize the killing ability of the dBTEs, we used recombinant BTEs in a 48-h killing assay with U87-GFP-Luc cells. We observed potent killing of U87-GFP-luc cells at extremely low doses of each dBTE. The EC_{50} value for each dBTE was approximately 100 pg/mL (Figure 3B).

We evaluated killing of 2 other GBM cell lines, U373 and U251, which express IL-13Rα2 at high levels (Figure S6), using the xCelligence system, which allows real-time monitoring of cytotoxicity over a period

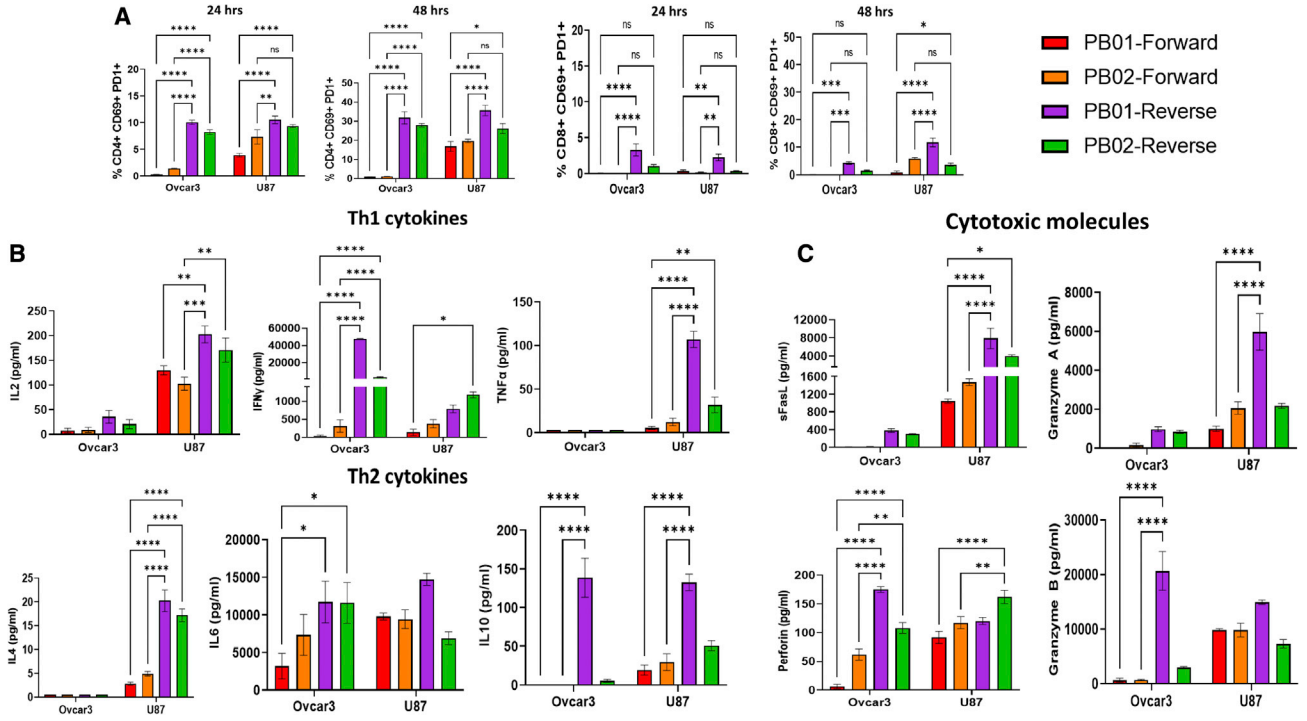

Figure 2. T cell activation in the presence of T cells and IL-13Rα2-expressing tumor cells

(A) Histogram plots showing percentages of CD4 and CD8 gated primary human T cells double-positive for PD-1 and CD69 as markers of T cell activation in the presence of dBTEs with or without U87 cells after 24 h and 48 h of co-culture. (B) Quantification of Th1 and Th2 cytokines secreted after 48 h of co-culture of dBTEs with primary human T cells in the presence or absence of U87 cells. (C) Quantification of the indicated cytotoxic molecules secreted after 48 h of co-culture of dBTEs with primary human T cells in the presence or absence of U87 cells. Ovcar3 cells were used as negative control cells (the concentration of supernatant in the final volume was 10%). All images represent the mean of 4 independent experiments using supernatant from 3 different transfections and 4 different T cell donors.

of several hours. We observed that both dBTEs in the forward orientation as well as those in the reverse orientation induced rapid killing of both cell lines; the EC_{50} values for U373 cells were between 3 and 8 ng/mL, and that for the U251 cell line was between 600 and 900 pg/mL (Figure 3C). To identify which T cell sub-population was responsible for cytolysis, we repeated the xCelligence killing assay with U87-GFP-luc as target cells. However, we used isolated $CD8^+$ or $CD4^+$ T cells as effector cells at an E:T ratio of 10:1. For all 4 dBTEs, we observed a trend of $CD8^+$ T cells killing target cells faster compared with $CD4^+$ T cells, and in the case of PB02-reverse dBTE, this difference was statistically significant (Figure 3D). These data suggest that the dBTEs can engage $CD8^+$ and $CD4^+$ T cells to kill target cells.

To ensure target-specific cytotoxicity, we performed a killing assay using the ovcar3 cell line. We observed potent killing of ovcar3 cells with dBTEs PB01-reverse and PB02-reverse and delayed but significant killing with PB02-forward as well (Figures S7A and S7B). We observed a strong correlation between the levels of granzyme B secretion and cytotoxicity. When co-cultured with U87 cells, all dBTEs induced similar levels of granzyme B, and all dBTEs induced comparable cytotoxicity of U87 cells. For the non-specific ovcar3 cells, the dBTEs in the reverse orientation induced significantly higher levels of granzyme B compared with dBTEs in the forward orientation. Similarly, dBTEs in the reverse orientation potently killed ovcar3 cells, and although PB02-forward induced some delayed killing, PB01-forward induced no killing of ovcar3 cells. These data support that PB01-forward exhibits high specificity and stringency without any off-target activity.

Based on these data, we selected PB01-forward as our lead candidate and decided to further evaluate the mechanism of its cytotoxicity. We repeated the killing assay with PB01-forward, but this time we added inhibitors for IFN-γ, TNF-α, FasL, TRAIL, or granzyme B at the indicated concentrations. Although we observed no effect of IFN-γ, TNF-α, FasL, or TRAIL inhibitors at 24 h or 48 h, granzyme B inhibition had a dose-dependent decrease in cytotoxicity at 24 h and 48 h (Figures 3E and S8). These data suggest that cytotoxicity induced by PB01-forward is dependent on the perforin/granzyme pathway.

dBTE has significantly enhanced *in vivo* persistence compared with recombinant BTE

To study the half-life of dBTEs *in vivo*, we injected immunodeficient NSG mice with DNA-encoded PB01-forward followed by electroporation or recombinant PB01-forward. We collected sera at the indicated time points and measured killing activity as a readout for levels of BTE in serum. We found that killing with recombinant BTE peaked

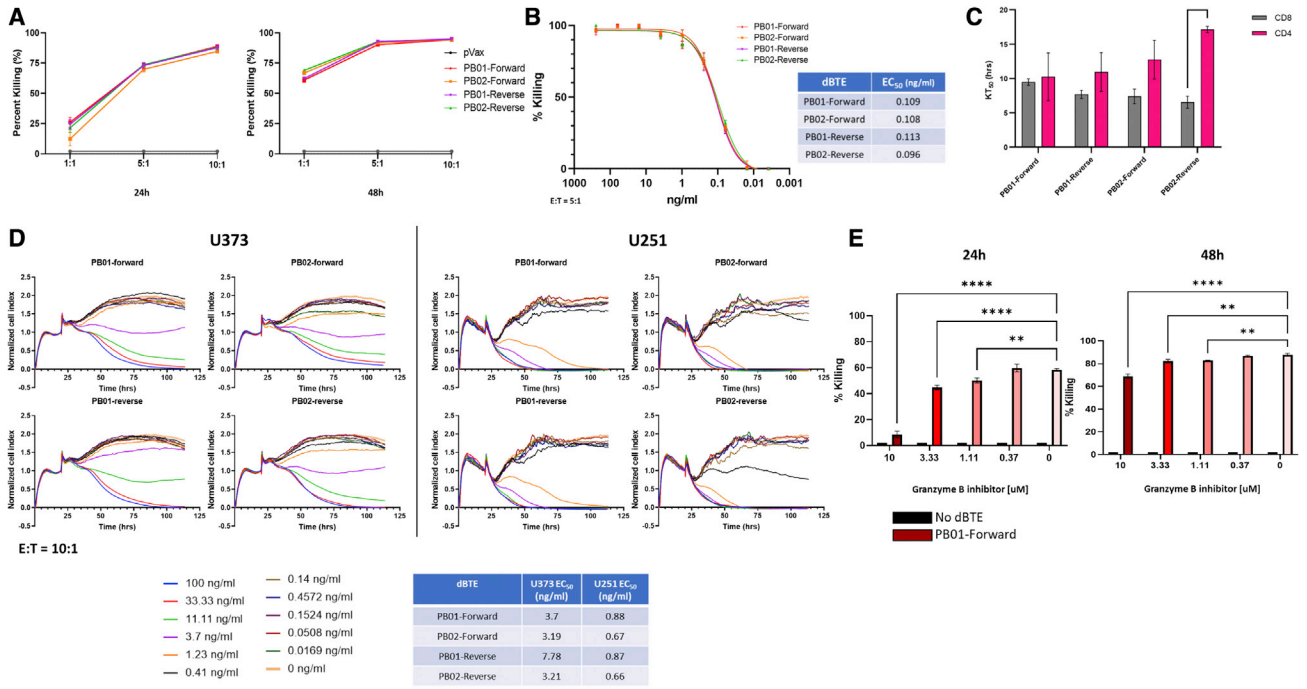

Figure 3. Cytotoxicity of target-expressing tumor cells in the presence of dBTEs and primary human T cells

(A) Percentage of killing of U87-GFP-luc cells, obtained by luciferase measurement when co-cultured with dBTEs and primary human T cells at the indicated E:T ratios and time points (the p value of pVax versus PB02-forward at a 1:1 ratio and at the 24-h time point is 0.051; for all other dBTEs at all E:T ratios and both time points, $p < 0.0001$). (B) Percentage of killing of U87-GFP-luc cells, obtained by luciferase measurement when co-cultured with recombinant BTEs at the indicated concentrations of each BTE at 48 h. (C) Normalized cell index plots showing dose-dependent killing by all dBTEs of U373 cells (left panel) and U251 cells (right panel). (D) Bar graphs showing KT_{50} (time to 50% killing) by all four dBTEs when cultured with purified CD4 or CD8 T cells. (E) Percentage of killing of U87-GFP-luc cells, obtained by luciferase measurement when co-cultured with PB01-forward at an E:T ratio of 5:1 in the presence of granzyme B inhibitor at the indicated concentrations. All data are representative of 3 separate experiments with 3 different T cell donors.

on day 3 and was quickly cleared from the sera by day 5. In contrast, killing from DNA-launched PB01-forward peaked on day 7, and we observed significant killing lasting until day 13. Peak killing from dBTE was much greater compared with recombinant BTE (Figure 4A). This suggests that DNA delivery not only leads to longer-term expression *in vivo* but also increases the absolute levels of BTE that can be achieved compared with recombinant BTE. We used a functional assay to quantify the amount of PB01-forward in the serum after injection. We found that PB01-forward reached a peak concentration of 103.1 ng/mL 4 days after injection. This starts to decline on day 7, and by day 21, we could not detect any dBTE in the animal serum (Figure 4B). In a separate experiment, we characterized the pharmacokinetic profile of dBTE using a flow cytometry-based T cell activation assay. We observed T cell activation as early as day 1 after injection, with activation peaking on day 5 and continued expression until day 19 (Figure 4C). Cytokine secretion upon co-culture of human T cells with sera from different time points and U87 cells also revealed a similar pK profile. All cytokines measured showed peak expression when co-cultured with sera from day 5, with detection of cytokines up to day 19 (Figure 4D). In another experiment, we cultured U87-GFP-luc cells with sera collected on the indicated days after injection of PB01-forward and primary human T cells at an E:T ratio of 10:1. We added the eCaspase 3 NucView 405 dye, which labels dead cells blue, to monitor killing of U87 cells. We observed that sera collected prior to dBTE injection (day 0) had no effect on the killing of U87 cells. In contrast, sera collected on day 8 after injection elicited strong and rapid killing, as evidenced by the rapid appearance of blue cells in the culture (Videos S1 and S2).

To validate the efficacy of PB01-forward in a different tumor model, we co-cultured supernatant from Expi293F cells transfected with PB01-forward with DaOY cells (a human neuroblastoma cell line that also expresses IL-13Rα2; Figure S9A) and human T cells. We observed a dose-dependent increase in cytotoxicity of DaOY cells with increasing concentration of supernatant in culture (Figure S9B). PB01-forward induced rapid killing of DaOY cells; it was able to kill over 80% of DaOY cells within 48 h of co-culture (Figure S9C). We also observed that sera from mice injected with PB01-Forward induced rapid killing of DaOY cells in an *in vitro* killing assay (Videos S3 and S4).

PB01-forward affects growth of subcutaneous U87 tumors *in vivo*

To study the efficacy of PB01-forward *in vivo*, we injected U87 cells into the right flank of NSG mice. 24 days after tumor injection, we injected mice with PB01-forward DNA followed by electroporation. We

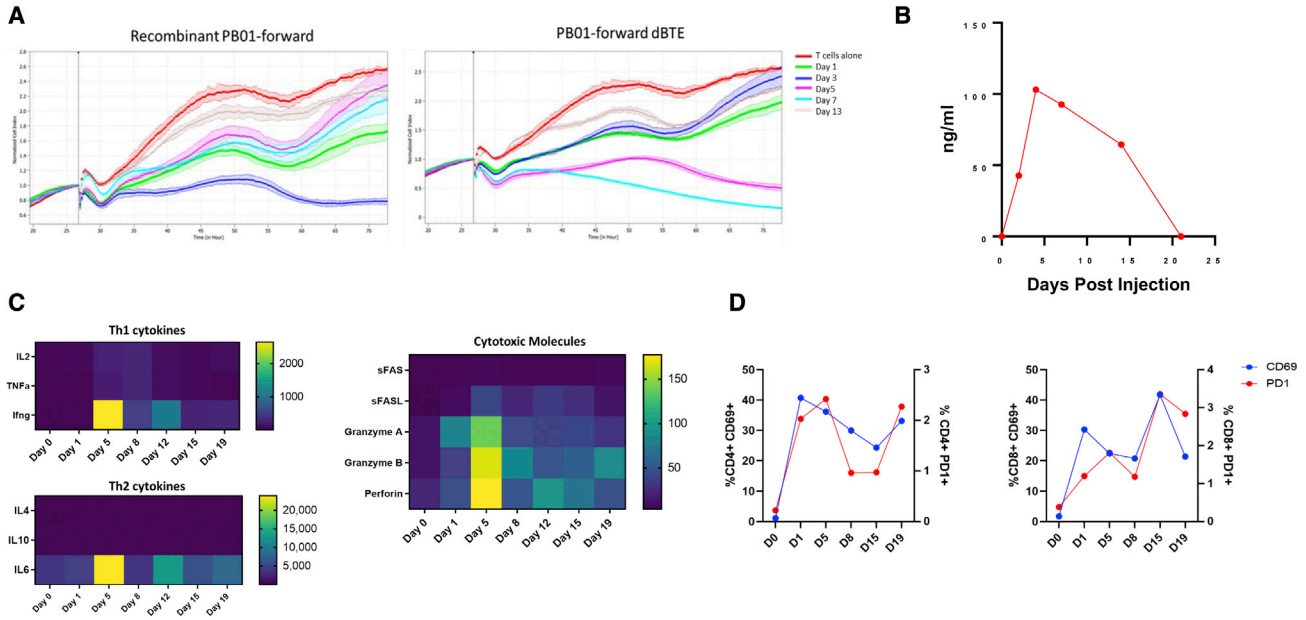

Figure 4. DNA-launched PB01-forward has significantly enhanced *in vivo* persistence compared with recombinant PB01-forward

(A) xCelligence-based killing assay of U87 cells using sera collected at the indicated time points from mice injected with recombinant (left) or DNA-launched PB01-forward. (B) Pharmacokinetic analysis of DNA-delivered PB01-forward in serum of NSG mice. (C) Quantification of Th1 and Th2 cytokines and cytotoxic molecules in 48-h supernatants of co-culture in (A) (all values in pg/mL). (D) Percentage of $CD69^+$ (left y axis) and percentage of $PD\text{-}1^+$ (right y axis) on CD4 and CD8 gated T cells after 48-h incubation with sera from mice immunized with PB01-forward and collected at the indicated time points and U87 cells (the concentration of serum in the final volume was 10%).

also injected 3e6 or 10e6 primary human T cells into the peritoneal cavity of mice on day 24. We gave the mice another dose of PB01-forward DNA on day 38 after tumor injection (Figure 5A). We observed that 100% of the mice receiving 10e6 T cells rejected tumor growth in the presence of PB01-forward compared with mice receiving pVax control DNA. 60% of the mice receiving 3e6 T cells also rejected tumor growth in presence of PB01-forward (Figure 5B). This treatment led to dramatically improved survival for the mice receiving PB01-forward regardless of whether they received 3e6 T cells or 10e6 T cells (Figure 5B). To rule out *in vivo* activation of T cells via binding to the anti-CD3 ScFv, which, in theory, can lead to tumor control, we repeated the tumor challenge using an irrelevant dBTE as the negative control (Figure S10A). In mice treated with the irrelevant dBTE, we observed no tumor control, and all mice rapidly grew tumors. All mice treated with PB01-forward completely controlled tumors, and we saw no evidence of tumor growth in these mice (Figure S10B). PB01-forward treatment also significantly enhanced the survival of mice compared with those treated with an irrelevant dTAB (Figure S10C). These data demonstrate that engagement of both arms of the BTE is required for T cell activation *in vivo*, which leads to specific cytolysis of target-expressing tumor cells.

We repeated the NSG tumor challenge with DaOY cells (Figure S11A). A single injection of PB01-forward controlled growth of DaOY tumors in the flank, demonstrating the efficacy of this lead dBTE in animal models of multiple different types of brain cancer (Figures S11B and S11C).

Peripherally delivered PB01-forward crosses the blood-brain barrier and affects U87 tumor growth in an intracranial model of GBM

To study the efficacy of PB01-forward in a clinically relevant setting, we used an orthotopic GBM model (Figure 6A). 3 days after tumor implantation, we injected the mice with PB01-forward DNA and 10e6 T cells. We performed IVIS-based imaging to follow tumor growth *in vivo*. With a single injection of PB01-forward DNA, we observed complete elimination of U87 tumors in 5 of 9 mice and slower growth of tumors in the remaining 4 mice (Figures 6B, 6C, and S11). This led to a significant reduction in total flux in mice treated with PB01-forward- compared with pVax-treated mice. We also followed body weight over time as a measure of disease progression. Mice treated with pVax lost weight much faster compared with those treated with PB01-forward (Figure 6D). The therapy also significantly extended the survival of mice with orthotopically implanted tumors (Figure 6E). In a separate cohort of 3 mice per group, mice were sacrificed on day 28, and their splenocytes were studied. We observed a significantly higher frequency of human $CD45^+$ cells in mice receiving PB01-forward compared with pVax-treated mice, suggesting BTE-mediated expansion of human T cells in these mice (Figure 6F). Further analysis showed that the ratio of CD4:CD8 cells was 2:1, which is the normal CD4:CD8 ratio in healthy humans (Figure 6G). This suggests that the dBTE can engage CD4 and $CD8^+$ T cells *in vivo* and that there is no preferential expansion of one sub-population over the other. These data support the hypothesis that the blood-brain barrier does not hinder

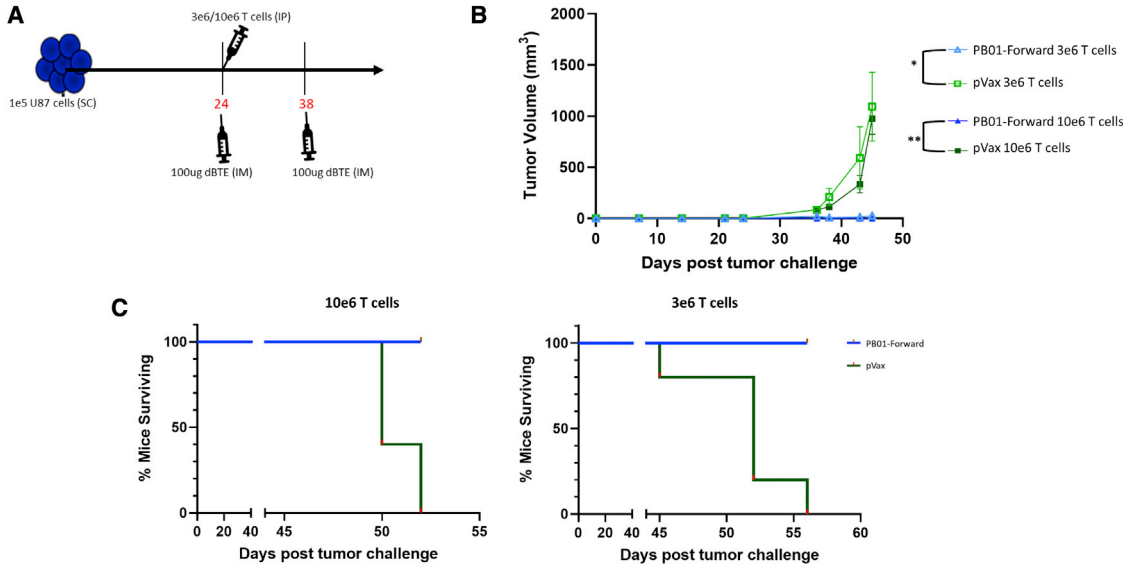

Figure 5. PB01-forward controls tumor growth *in vivo* and extends the survival of tumor-bearing mice

(A) Schematic explaining the experimental timeline in (B) and (C). (B) Mean tumor volume of mice injected with U87 cells and treated with PB01-forward (blue triangles) or pVax empty vector control (green squares). Darker lines represent mice treated with 10e6 primary human T cells, and lighter lines indicate mice treated with 3e6 primary human T cells. (C) Survival proportion of mice injected with U87 cells and treated with PB01-forward (blue) or pVax (green) and primary human T cells (n = 5 mice/group). Graphs are representative of two separate experiments done with two different T cell donors.

the ability of peripherally delivered dBTE to control tumor growth in the brain.

DISCUSSION

Bispecific antibodies have shown remarkable effects in hematological cancers, leading to FDA approval of a new therapeutic agent for the treatment of ALL.[5] The recent approval of a bispecific antibody for treatment of metastatic non-small cell lung cancer suggests that bispecific antibodies can be an important therapeutic intervention for solid tumors as well.[23] Non-specific, off-target binding and CRS, which is caused by excessive cytokine secretion, remain major challenges for CD3-engaging bispecific antibodies.[6]

In our study, all dBTEs bound specifically to IL-13Rα2 with equal affinity, and no binding was observed to IL-13Rα1 in a recombinant form or when expressed on tumor cells. However, dBTEs in the reverse (V_H-V_L-V_L-V_H) orientation had significantly higher affinity toward CD3 compared with those in the forward (V_L-V_H-V_H-V_L) orientation. This fine-tuning had major implications for specificity and function because dBTEs in the forward orientation had significantly lower levels of T cell activation and cytokine secretion in the presence of IL-13Rα2$^+$ as well as IL-13Rα2$^-$ tumors compared with dBTEs in the reverse orientation. We also observed significant off-target toxicity from dBTEs with the reverse orientation compared with the forward orientation, supporting the hypothesis that the orientation of heavy and light chains in bispecific antibodies can have a significant effect on off-target toxicity. Based on these findings, the PB01-forward BTE was studied further. A single injection of DNA delivery of PB01-forward significantly enhanced expression levels and time of expression *in vivo* compared with recombinant BTE. In a subcutaneous *in vivo* tumor challenge, 100% of mice treated with the lead dBTE were able to reject tumor growth compared with a group treated with a plasmid vector control. Finally, we observed that systemically delivered PB01-forward crosses the blood-brain barrier and controlled GBM tumors in an orthotopic setting, allowing enhanced survival of mice.

In functional assays, all four dBTEs activated CD4 and CD8 T cells in the presence of U87 cells, but those in the reverse orientation also induced T cell activation in the presence of ovcar3 cells. dBTEs in the reverse orientation also generally induced higher levels of cytokines and cytotoxic granule secretion in the presence of U87 cells. In the presence of ovcar3 cells, however, dBTEs in the reverse orientation induced significantly higher levels of cytokine secretion, especially IFN-γ, IL-6, and IL-10. They also induced significantly higher levels of perforin and granzyme B in the presence of ovcar3 cells compared with dBTEs in the forward orientation. The levels of secreted perforin/granzyme B directly correlated with the levels of cellular cytotoxicity. Although we observed no differences in the specific killing of U87, U251, or U373 cells, the dBTEs in the reverse orientation induced strong non-specific killing of ovcar3 cells. PB02-forward, which induced intermediate levels of perforin, had delayed but significant non-specific killing of ovcar3 cells. PB01-forward, which induced no secretion of granzyme B/perforin in the presence of ocvar3 cells, induced no killing of ovcar3 cells. The fact that PB01-forward also induced the least amounts of cytokine secretion (in the presence of targeting expressing as well as non-expressing cell lines) suggests that PB01-forward has the lowest risk for CRS

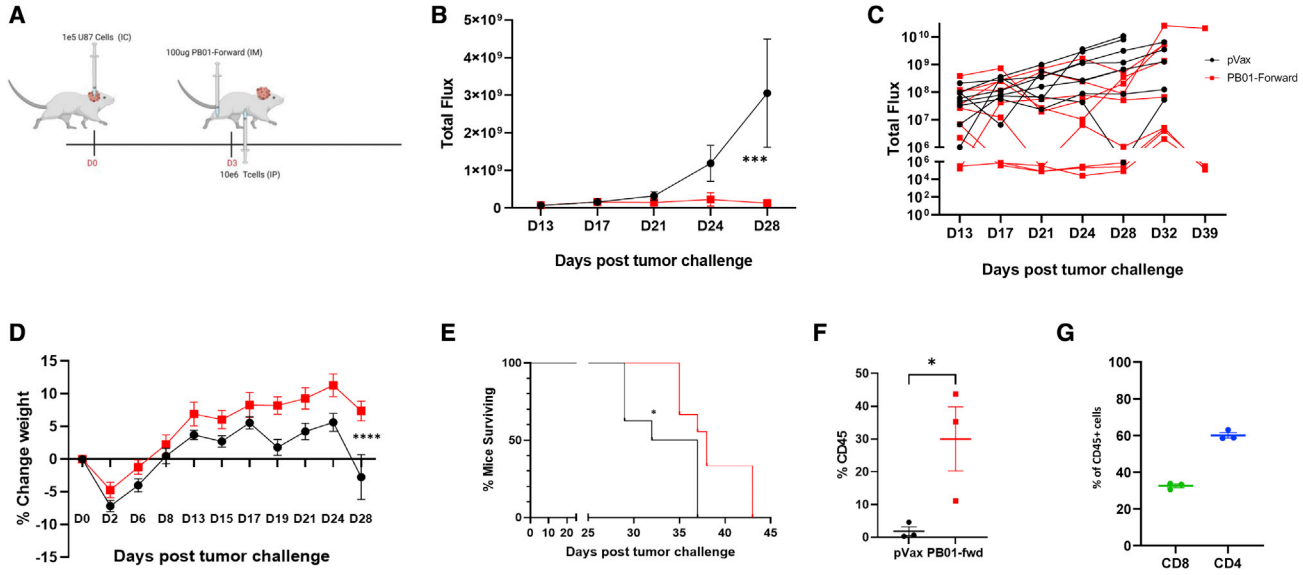

Figure 6. PB01-forward crosses the blood-brain barrier and controls U87 tumors in an orthotopic GBM model

(A) Schematic explaining the experimental timeline for the orthotopic GBM model. (B) Mean total flux in mice, representing the tumor burden in mice with an intracranial tumor implant and treated with pVax (black circles) or PB01-forward (red boxes) and 10e6 primary human T cells. (C) Total flux of individual mice (groups as in B). (D) Mean change in weight of mice after U87 tumor implantation after treatment with pVax (black circles) or PB01-forward (red boxes) and 10e6 primary human T cells. (E) Survival proportion of mice, suggesting increased survival of mice treated with pVax or PB01-forward and 10e6 T cells (n = 8 or 9 mice/group). (F) Percentage of human $CD45^+$ splenocytes in mice implanted with orthotopic U87 tumors and treated with pVax or PB01-forward (n = 3 mice/group). (G) Percentage of CD8 and CD4 T cells in the $CD45^+$ fraction in (F).

induction. We posit that the higher affinity toward CD3 of dBTEs in the reverse orientation allows easier activation of T cells, which leads to increased granzyme B secretion and enhanced killing of ovcar3 cells. In contrast, the lower CD3 affinity of dBTEs in the forward orientation limits T cell activation to when dBTE also engages IL-13Rα2 on tumors, limiting granzyme B secretion and reduced or no killing of ovcar3 cells. Further studies will be required to better elucidate the exact mechanisms of T cell activation by dBTEs in the reverse orientation in the absence of IL-13Rα2-expressing cell lines.

Multiple factors have been reported to affect cytokine secretion and cytotoxicity induced by dBTEs. Bortoletto et al.[24] showed that a bispecific antibody with lower CD3 affinity led to lower T cell activation and lower killing of target cells. Several groups have reported the benefits of lower CD3 affinity for bispecific antibodies; they observed lower cytokine secretion *in vivo* without compromising the ability to control tumors.[25–27] Our study adds to this body of work and shows that the binding affinity to CD3 can significantly affect non-specific toxicity induced by bispecific antibodies while having a minimal effect on the specific killing induced by the bispecific antibodies. To the best of our knowledge, this is the first study to compare the effect of binding affinity to CD3 and the role of heavy- and light-chain orientation of scFv on specific and non-specific toxicity induced by bispecific antibodies. The strong correlation observed with secretion of granzyme B/perforin suggests that this could be a useful tool for future screening of such biologic agents to study non-specific toxicity induced by antibody-based therapeutic agents, such as bispecific antibodies and CAR T cells.

Another issue limiting the development of bispecific antibody therapies is the short half-life, which requires continuous intravenous (i.v.) infusion over a period of several days.[7] A simplified delivery system with better pK would improve the feasibility of using bispecific antibody technology and make it available to a wider group of affected individuals. DNA-encoded monoclonal antibodies are a new technology with appealing biological characteristics. Recent publications have described expression with effects on disease; i.e., control of tumors or infection challenge.[28–30] DNA-encoded bispecific antibodies have been shown to be expressed for several months *in vivo* and have demonstrated tumor control in an animal model of ovarian cancer.[8] Pituch et al.[31] tried to address the short half-life by using modified neural stem cells (NSCs) as bispecific T cell engager (BiTE)-secreting entities. By modifying NSCs to secrete an IL-13Rα2-targeting BiTE, they were able to improve the survival of tumor-bearing mice by 1 week. The NSCs, however, were cleared rapidly, suggesting that repeat administration would be required to see a sustained therapeutic effect.[31] This was also seen by another group that used an EGFRviii-targeting BiTE that required daily administration to improve animal survival in an orthotopic model of GBM.[32] In our study, a single DNA injection of PB01-forward provided long-term expression compared with recombinant PB01-forward. This peripherally delivered dBTE significantly controlled GBM tumor growth in an orthotopic setting. At the end of the study, 3 of 4 surviving mice had no detectable tumor burden based on bioluminescence imaging. However, this is not a perfect model for long-term studies because the mice develop graft versus host disease (GvHD) from the transfer of human T cells into a mouse.[33–36] Therefore, the

more effective the treatment, the more likely it is that the mice will succumb to GvHD and not the tumor burden. GvHD necessitates sacrificing the mice when symptoms present despite no detectable tumor burden in these mice. This explains why mice treated with PB01-forward survived only an additional week compared with the control mice. The peripherally delivered dBTE can reach the brain tumor independently, or it can first bind to T cells in the periphery, which then carry the dBTE across the blood-brain barrier. Further studies will be required to elucidate the exact pathway of how the dBTE reaches the brain tumor site.

Besides GBM, IL-13Rα2 is also upregulated in other cancer types, such as medulloblastoma, advanced melanoma, head and neck cancers, as well as ovarian cancers.[37–40] We already have preliminary data showing that our dBTE can be effective in the treatment of medulloblastoma. These data support the hypothesis that dBTEs can be a valuable addition to the toolbox for immunotherapies against GBM and enhance therapeutic options for a variety of cancers. IL-13Rα2 has also been implicated in sunitinib resistance in clear cell renal cell carcinoma,[41] which implies that our dBTE could provide clinical benefits to individuals who do not respond to or eventually progress on sunitinib therapy. The design orientation that was most effective and specific in our hands might be important in the development of similar reagents for other cancers and infectious diseases. Fine-tuning BTE function by studying the effect of arrangement of heavy and light chains on could be important for CAR T cells and other biologic agents. Further study for possible development and optimization of these new therapeutic agents for GBM is warranted.

MATERIALS AND METHODS

Animals and cell lines

NSG mice were purchased from The Wistar Institute animal facility. The U87 and DaOY cell lines were purchased from the ATCC. The U373 and U251 cell lines were purchased from Sigma-Aldrich. Ovcar3 cells were provided by Dr. Conejo-Garcia (Department of Immunology, Moffit Cancer Center, Tampa, FL). Primary human T cells were derived from healthy donors by the Human Immunology Core at the University of Pennsylvania. All animal experiments were done with approval from the Institutional Animal Care and Use Committee at The Wistar Institute.

dBTE design

The heavy- and light-chain sequences were derived from humanized antibodies as described previously.[19] We fused the heavy and light chains of IL-13Rα2-targeting antibodies to heavy and light chains of a modified UCHT1 antibody via GS linkers. All sequences were codon optimized and encoded in a non-replicating pVax vector (Figure 1A). The sequences of all four BTEs are as follows:

PB01-forward, 5′-MDWTWILFLVAAATRVHSDIQMTQSPSSLSASVGDRVTITCTASLSVSSTYLHWYQQKPGSSPKLWIYSTSNLASGVPSRFSGSGSGTSYTLTISSLQPEDFATYYCHQYHRSPLTFGGGTKVEIKGGGGSGGGGSGGGGSEVQLVESGGGLVQPGGSLRLSCAASGFSLTKYGVHWVRQAPGKGLEWVGVKWAGGSTDYNSALMSRFTISKDNAKNSLYLQMNSLRAEDTAVYYCARDHRDAMDYWGQGTLVTVSSGGGGSEVQLVESGGGLVQPGGSLRLSCAASGYSFTGYTMNWVRQAPGKGLEWVALINPYKGVSTYNQKFKDRFTISVDKSKNTAYLQMNSLRAEDTAVYYCARSGYYGDSDWYFDVWGQGTLVTVSSGGGGSGGGGSGGGGSDIQMTQSPSSLSASVGDRVTITCRASQDIRNYLNWYQQKPGKAPKLLIYYTSRLESGVPSRFSGSGSGTDYTLTISSLQPEDFATYYCQQGNTLPWTFGQGTKVEIKS-3′; PB01-reverse, 5′-MDWTWILFLVAAATRVHSEVQLVESGGGLVQPGGSLRLSCAASGFSLTKYGVHWVRQAPGKGLEWVGVKWAGGSTDYNSALMSRFTISKDNAKNSLYLQMNSLRAEDTAVYYCARDHRDAMDYWGQGTLVTVSSGGGGSGGGGSGGGGSDIQMTQSPSSLSASVGDRVTITCTASLSVSSTYLHWYQQKPGSSPKLWIYSTSNLASGVPSRFSGSGSGTSYTLTISSLQPEDFATYYCHQYHRSPLTFGGGTKVEIKGGGGSDIQMTQSPSSLSASVGDRVTITCRASQDIRNYLNWYQQKPGKAPKLLIYYTSRLESGVPSRFSGSGSGTDYTLTISSLQPEDFATYYCQQGNTLPWTFGQGTKVEIKSGGGGSGGGGSGGGGSEVQLVESGGGLVQPGGSLRLSCAASGYSFTGYTMNWVRQAPGKGLEWVALINPYKGVSTYNQKFKDRFTISVDKSKNTAYLQMNSLRAEDTAVYYCARSGYYGDSDWYFDVWGQGTLVTVSS-3′; PB02-forward, 5′-MDWTWILFLVAAATRVHSDIQMTQSPSSLSASVGDRVTITCKASQDVGTAVAWYQQKPGKAPKLLIYSASYRSTGVPSRFSGSGSGTDFTLTISSLQPEDFATYYCQHHYSAPWTFGGGTKVEIKGGGGSGGGGSGGGGSEVQLVESGGGLVQPGGSLRLSCAASGFTFSRNGMSWVRQAPGKGLEWVATVSSGGSYIYYADSVKGRFTISRDNAKNSLYLQMNSLRAEDTAVYYCARQGTTALATRFFDVWGQGTLVTVSSGGGGSGGGGSGGGGSDIQMTQSPSSLSASVGDRVTITCRASQDIRNYLNWYQQKPGKAPKLLIYYTSRLESGVPSRFSGSGSGTDYTLTISSLQPEDFATYYCQQGNTLPWTFGQGTKVEIKSGGGGSGGGGSGGGGSEVQLVESGGGLVQPGGSLRLSCAASGYSFTGYTMNWVRQAPGKGLEWVALINPYKGVSTYNQKFKDRFTISVDKSKNTAYLQMNSLRAEDTAVYYCARSGYYGDSDWYFDVWGQGTLVTVSS-3′. and PB02-reverse, 5′-MDWTWILFLVAAATRVHSEVQLVESGGGLVQPGGSLRLSCAASGFTFSRNGMSWVRQAPGKGLEWVATVSSGGSYIYYADSVKGRFTISRDNAKNSLYLQMNSLRAEDTAVYYCARQGTTALATRFFDVWGQGTLVTVSSGGGGSGGGGSGGGGSDIQMTQSPSSLSASVGDRVTITCKASQDVGTAVAWYQQKPGKAPKLLIYSASYRSTGVPSRFSGSGSGTDFTLTISSLQPEDFATYYCQHHYSAPWTFGGGTKVEIKGGGGSDIQMTQSPSSLSASVGDRVTITCRASQDIRNYLNWYQQKPGKAPKLLIYYTSRLESGVPSRFSGSGSGTDYTLTISSLQPEDFATYYCQQGNTLPWTFGQGTKVEIKSGGGGSGGGGSGGGGSEVQLVESGGGLVQPGGSLRLSCAASGYSFTGYTMNWVRQAPGKGLEWVALINPYKGVSTYNQKFKDRFTISVDKSKNTAYLQMNSLRAEDTAVYYCARSGYYGDSDWYFDVWGQGTLVTVSS-3′.

Immunoblotting

Denaturation and western blotting were done as described previously.[8] Supernatant from Expi293F cells was transfected with dBTE encoding DNA was run on the gel. Goat anti-human Fab fragment-specific antibody (Jackson ImmunoResearch) was used to detect the dBTEs, and anti-goat antibody (LI-COR Biosciences) was used as a secondary antibody. Images were taken using Odyssey-Clx (LI-COR Biosciences).

Flow cytometry

IL-13Rα2 expression on tumor cells was checked using a commercially available antibody (BioLegend, catalog number 354404). To detect binding of dBTEs to IL-13Rα2 and CD3, supernatants from Expi293F-transfected cells were incubated with U87 cells and primary human T cells, respectively. Fluorophore-conjugated goat anti-human Fab fragment-specific antibody (Jackson ImmunoResearch) was used as a secondary antibody. Data were acquired on LSR Fortessa (BD Biosciences). Images are representative of 4 independent transfections. For the T cell activation assay, CD4 (OKT4), CD8 (SK1), CD69 (FN50), and PD-1 (EH12.2H7), all from BioLegend, were used. Dead cells were excluded using Live-Dead viability dye (Invitrogen).

Binding ELISA

We coated ELISA plates with IL-13Rα2/IL-13Rα1 (Sino Biological, 1 μg/mL) or CD3 (Acrobiosystems, 1 μg/mL) overnight at 4°C. We blocked with PBST-10% fetal bovine serum (FBS) for 1 h. As primary antibody we used supernatants from Expi293F cells transfected with dBTEs or pVax as a negative control at different dilutions. We incubated at room temperature for 1 h. The secondary antibody was a goat anti-human Fab fragment-specific horseradish peroxidase (HRP)-conjugated antibody (Jackson ImmunoResearch). After 1-h incubation, we developed with TMB solution and read the optical density (OD) at 450 nm. To determine binding kinetics, we used recombinant BTEs at the indicated concentrations as primary antibody and HRP-conjugated anti-His tag antibody (BioLegend) or goat anti-mouse Fab fragment-specific antibody as secondary antibody.

Surface plasmon resonance

The affinity of dBTEs to IL-13Rα2 was assessed using a Biacore T200 SPR instrument. Recombinant, purified BTE with a His_6 tag was used for this experiment. Briefly, anti-His antibodies (THE HIS antibody, Genscript) was immobilized on a carboxymethyl dextran sensor chip (CMD200L, Xantec Bioanalytics) by amine coupling. The chip was first washed with 1 M NaCl, 0.1 M sodium borate (pH 9.0) for 3 min at 10 μL/min, followed by activation with 25 mM EDC (N-(3-dimethylaminopropyl)-N′-ethyl carbodiimide hydrochloride), 100 mM NHS (N-hydroxy succinimide ester) for 12 min at 10 μL/min. The anti-His antibodies were then flowed over the chip in 10 mM sodium acetate (pH 5.0) at 10 μg/mL for 5 min. After 30 min of washing with distilled water, the remaining activated sites were blocked with 1 M Tris (pH 7.4) for 5 min at 10 μL/min. After immobilization of the anti-His antibodies, the running buffer was changed from distilled water to 10 mM HEPES (pH 7.4), 150 mM NaCl, 0.05% Tween 20. Approximately 200–300 RU of IL-13a2 antibodies was captured on flow cells 2, 3, and 4 by flowing over ~8 μg/mL antibody at 10 μL/min for 30 s. Flow cell 1 was left blank (anti-His antibody alone) as a reference. IL-13a2 was serially diluted 1:2 from 0–400 nM; the association time was 4 min, and the dissociation time was 12 min at a flow rate of 30 μL/min. After each injection of IL-13a2, the antibody/antigen complex was completely dissociated using 20 mM glycine (pH 2.0). The resulting sensograms were analyzed by global nonlinear regression of a one-site kinetic binding model using the Biacore Evaluation software.

Competition ELISA

We coated ELISA plates with IL-13Rα2 (Sino Biological, 1 μg/mL) overnight at 4°C. We blocked with PBST-10% FBS for 1 h. Next we pre-incubated with supernatants of Expi293F cells transfected with PB01-forward, PB01-reverse, PB02-forward, or PB02-reverse for 1 h at room temperature. We then added recombinant, purified versions of all four dBTEs that had been modified to contain a His_6 tag. We then used an HRP-conjugated anti-His tag antibody (BioLegend) to detect binding of recombinant BTEs to IL-13Rα2. Finally we developed with TMB solution and read the OD at 450 nm.

Cytokine secretion

Supernatants from co-cultures with primary human T cells and dBTEs in the presence of U87 or ovcar3 tumors were collected. In another experiment, U87 cells were co-cultured with sera from mice immunized with PB01-forward and primary human T cells, and supernatants were collected at 48 h. The cytokines were quantified using the BioLegend Legendplex assay according to the manufacturer's instructions. All conditions were tested in duplicate, and mean cytokine concentrations are reported. The human CD8/NK panel was used for cytokine evaluation.

Cytotoxicity assay

U87 cells were transfected with a lentivirus to make them express GFP and luciferase (U87-GFP-luc). The U87-GFP-luc cell line was co-cultured with supernatants from dBTE-transfected Expi293F cells and primary human T cells at the indicated ratios. The final concentration of dBTE supernatant in the assay was 10%. After 24-h or 48-h incubation, we lysed the cells and measured luciferase expression using CytoTox Glo (Promega). Cytotoxicity was calculated as (maximum viability control – individual well)/(maximum viability control – maximum death control) × 100 as a percentage. All experiments were done in triplicates, and figure is mean of 4 independent experiments with 4 different T cell donors. To determine killing kinetics, recombinant dBTEs at the indicated concentrations were used.

To determine the mechanism of cytotoxicity, neutralizing antibodies against IFN-γ (506532), TNF-α (502805), TRAIL (208213) (all from BioLegend) and FasL (556317, BD Pharmingen) were added at the indicated concentrations. Granzyme B activity was inhibited using granzyme B inhibitor 1 (Millipore Sigma) at the indicated concentrations.

xCelligence killing assay

The cytotoxicity of target cells was evaluated using the xCelligence Real-Time Cell Analyzer System (ACEA Biosciences). We plated tumor cells (1e4 cells/well). The next day, T cells and supernatant from dBTE-transfected Expi293F cells were added at the indicated E:T ratios and concentrations of dBTE supernatant. The cell index was monitored every 20 min and normalized to the maximum cell index value immediately prior to T cell addition. The percentage of

cytotoxicity and KT_{50} and KT_{80} values were calculated using the RTCA immunotherapy software. In some experiments, serum from NSG mice injected with 100 μg of DNA encoding PB01-forward and 40 U hyaluronidase and collected at different time points after injection was used instead of dBTE supernatant.

dBTE quantification in mouse serum

We used recombinant PB01-forward at varying doses in a luminescence-based killing assay to establish a standard curve. We also included serum from mice injected with PB01-forward DNA collected at indicated time points in this assay. We quantified the level of PB01-forward by comparing the killing induced by serum with the standard curve established using recombinant PB01-forward.

Subcutaneous *in vivo* tumor challenge

1e5 U87 cells were injected into the right flank of NSG mice. 24 days later, mice were injected with 100 μg of DNA encoding PB01-forward and 40 U hyaluronidase in the tibialis anterior (TA) muscle, followed by electroporation with the CELLECTRA device (Inovio). They were also given 10e6 or 3e6 primary human T cells via intraperitoneal injection. Mice were re-injected with 100 μg DNA encoding PB01-forward and 40 U hyaluronidase, followed by electroporation on day 38. The tumor size was measured using calipers, and tumor volume was calculated using the formula $V = ([\text{length} \times \text{width}^2] \times 3.14)/2$, where width is considered the side with the smaller measurement. Mice were sacrificed when they reached the predetermined endpoint value in accordance with IACUC protocols. Figure is representative of 2 independent experiments done with 2 different T cell donors.

For DaOY tumor challenge, 5e6 DaOY cells were injected into the right flank of NSG mice. 2 weeks after tumor implantation, mice were injected with 100 μg of DNA encoding PB01-forward and 40 U hyaluronidase, followed by electroporation. They were also given 10e6 primary human T cells via intraperitoneal injection.

Orthotopic tumor challenge

To generate the orthotopic brain tumor model, NSG mice were surgically implanted with U87-luc cells. Cells were brought to a concentration of 100,000 cells in 2 μL PBS. Mice were anesthetized using a ketamine/xylazine cocktail for surgeries. A midline scalp incision was made, and a burr hole was drilled 1 mm posterior to the bregma and 2 mm lateral to the midline. A 2-μL Hamilton syringe was lowered to a depth of 2.5 mm, and 2 μL of cell solution was injected over 2 min using an automated syringe pump mounted to a mouse stereotaxic frame. The syringe was then withdrawn slowly over 10 min. The incision was sutured, and antibiotic cream and the analgesic buprenorphine were applied. 3 days after tumor implantation, mice were injected with 100 μg of DNA encoding PB01-forward and 40 U hyaluronidase in the TA muscle, followed by electroporation. They were also given 10e6 primary human T cells via intraperitoneal injection. *In vivo* imaging using IVIS was used to follow tumor growth over time. The mice were sacrificed at a predetermined experimental endpoint. For analysis of spleens, 3 mice per group were sacrificed and their splenocytes isolated. The splenocytes were stained for human $CD45^+$, $CD8^+$, and $CD4^+$ cells to gauge T cell levels in these mice.

In vivo luminescence imaging

Mice were injected intraperitoneally (i.p.) with 3 mg of D-luciferin in 200 μL PBS. After 10 min, mice were imaged on a Xenogen IVIS Spectrum CT for luminescence. All settings were kept constant for all mice at all time points. Quantification of the tumor signal was performed using LivingImage software by defining a region of interest around the brain tumor and measuring total flux.

Statistics

In vitro cytotoxicity at 24 and 48 h was compared using 2-way ANOVA with Dunnett's multiple comparisons test. Each experiment was done in triplicate unless otherwise indicated, and error bars represent SEM. Tumor sizes were compared using 2-way ANOVA, and error bars represent SEM. Animal survival was compared using a log rank test.

Cytotoxicity using serum from immunized mice

NSG mice were injected with 100 μg DNA encoding PB01-forward and 40 U hyaluronidase in the TA muscle, followed by electroporation, and serum was collected at the indicated time points. 1e4 U87-GFP-luc cells were plated in an eSight plate (Agilent). After overnight incubation, sera collected at different time points were added to the cells along with primary human T cells at an E:T ratio of 5:1. eCaspase 3 NucView 405 (Agilent) was added to the wells to label dead cells blue. Images were taken using xCelligence eSight at 3-h intervals for a total duration of 81 h. Images from just before addition of effector cells up to the end of the experiment were used to create the videos using the xCelligence eSight data analysis software (Agilent). For comparison with recombinant BTE, NSG mice were given a single i.v. infusion of recombinant PB01-forward (0.5 mg/kg). This dose was chosen based on the highest dose of recombinant EGFRviii BTE used in a similar orthotopic GBM model.[32]

DATA AVAILABILITY

All data are available in the main text or supplemental information.

SUPPLEMENTAL INFORMATION

Supplemental information can be found online at https://doi.org/10.1016/j.omto.2022.07.003.

ACKNOWLEDGMENTS

We thank the animal facility staff at The Wistar Institute for providing care to the animals. We thank the Wistar Flow Core for assistance with the flow cytometry experiments. Funding support for The Wistar Institute core facilities was provided by Cancer Center support grant P30 CA010815. This work was supported in part by internal research funding from INOVIO Pharmaceuticals (to D.B.W.). D.B.W is supported in part by the W.W. Smith Charitable Trust Professorship in cancer research.

AUTHOR CONTRIBUTIONS

P.S.B. and D.B.W. conceptualized the study and designed the experiments. P.S.B., R.P.O., D.P., A.R.A., D.B., J.C., N.J.T., E.G., and K.L. performed experiments and acquired and analyzed the data. All authors contributed to writing and revision of the manuscript.

DECLARATION OF INTERESTS

D.B.W. discloses the following paid associations with commercial partners: GeneOne (consultant), Geneos (advisory board, research funding, stock), AstraZeneca (advisory board, speaker), Inovio (BOD, SRA, stock), Pfizer (speaker), Merck (speaker), Sanofi (advisory board), and BBI (advisory board).

REFERENCES

1. Brown, C.E., Aguilar, B., Starr, R., Yang, X., Chang, W.C., Weng, L., Chang, B., Sarkissian, A., Brito, A., Sanchez, J.F., et al. (2018). Optimization of IL13Ra2-targeted chimeric antigen receptor T cells for improved anti-tumor efficacy against glioblastoma. Mol. Ther. *26*, 31–44.
2. Stupp, R., Mason, W.P., van den Bent, M.J., Weller, M., Fisher, B., Taphoorn, M.J.B., Belanger, K., Brandes, A.A., Marosi, C., Bogdahn, U., et al. (2005). Radiotherapy plus concomitant and adjuvant temozolomide for glioblastoma. N. Engl. J. Med. *352*, 987–996.
3. Dolecek, T.A., Propp, J.M., Stroup, N.E., and Kruchko, C. (2012). CBTRUS statistical report: primary brain and central nervous system tumors diagnosed in the United States in 2005–2009. Neuro. Oncol. *14*, v1–v49.
4. Bi, W.L., and Beroukhim, R. (2014). Beating the odds: extreme long-term survival with glioblastoma. Neuro. Oncol. *16*, 1159–1160.
5. Jen, E.Y., Xu, Q., Schetter, A., Przepiorka, D., Shen, Y.L., Roscoe, D., Sridhara, R., Deisseroth, A., Philip, R., Farrell, A.T., et al. (2019). FDA approval: blinatumomab for patients with B-cell precursor acute lymphoblastic leukemia in morphologic remission with minimal residual disease. Clin. Cancer Res. *25*, 473–477.
6. Teachey, D.T., Rheingold, S.R., Maude, S.L., Zugmaier, G., Barrett, D.M., Seif, A.E., Nichols, K.E., Suppa, E.K., Kalos, M., Berg, R.A., et al. (2013). Cytokine release syndrome after blinatumomab treatment related to abnormal macrophage activation and ameliorated with cytokine-directed therapy. Blood *121*, 5154–5157.
7. Zhu, M., Wu, B., Brandl, C., Johnson, J., Wolf, A., Chow, A., and Doshi, S. (2016). Blinatumomab, a bispecific T-cell engager (BiTE®) for CD-19 targeted cancer immunotherapy: clinical pharmacology and its implications. Clin. Pharmacokinet. *55*, 1271–1288.
8. Perales-Puchalt, A., Duperret, E.K., Yang, X., Hernandez, P., Wojtak, K., Zhu, X., Jung, S.H., Tello-Ruiz, E., Wise, M.C., Montaner, L.J., et al. (2019). DNA-encoded bispecific T cell engagers and antibodies present long-term antitumor activity. JCI Insight *4*, 126086.
9. Tabata, Y., and Khurana Hershey, G.K. (2007). IL-13 receptor isoforms: breaking through the complexity. Curr. Allergy Asthma Rep. *7*, 338–345.
10. Hershey, G.K.K., and Khurana, G.K. (2003). IL-13 receptors and signaling pathways: an evolving web. J. Allergy Clin. Immunol. *111*, 677–690. quiz 691.
11. Brown, C.E., Warden, C.D., Starr, R., Deng, X., Badie, B., Yuan, Y.C., Forman, S.J., and Barish, M.E. (2013). Glioma IL13Rα2 is associated with mesenchymal signature gene expression and poor patient prognosis. Plos One *8*, e77769.
12. Brown, C.E., Starr, R., Aguilar, B., Shami, A.F., Martinez, C., D'Apuzzo, M., Barish, M.E., Forman, S.J., and Jensen, M.C. (2012). Stem-like tumor initiating cells isolated from IL13Rα2-expressing gliomas are targeted and killed by IL13-zetakine redirected T cells. Clin. Cancer Res. *18*, 2199–2209.
13. Mintz, A., Gibo, D.M., Slagle-Webb, B., Christensen, N.D., and Debinski, W. (2002). IL-13Ralpha2 is a glioma-restricted receptor for interleukin-13. Neoplasia *4*, 388–399.
14. Thaci, B., Brown, C.E., Binello, E., Werbaneth, K., Sampath, P., and Sengupta, S. (2014). Significance of interleukin-13 receptor alpha 2-targeted glioblastoma therapy. Neuro. Oncol. *16*, 1304–1312.
15. Debinski, W., Gibo, D.M., Slagle, B., Powers, S.K., and Gillespie, G.Y. (1999). Receptor for interleukin 13 is abundantly and specifically over-expressed in patients with glioblastoma multiforme. Int. J. Oncol. *15*, 481–486.
16. Sattiraju, A., Solingapuram Sai, K.K., Xuan, A., Pandya, D.N., Almaguel, F.G., Wadas, T.J., Herpai, D.M., Debinski, W., and Mintz, A. (2017). IL13RA2 targeted alpha particle therapy against glioblastomas. Oncotarget *8*, 42997–43007.
17. Iwami, K., Shimato, S., Ohno, M., Okada, H., Nakahara, N., Sato, Y., Yoshida, J., Suzuki, S., Nishikawa, H., Shiku, H., et al. (2012). Peptide-pulsed dendritic cell vaccination targeting interleukin-13 receptor a 2 chain in recurrent malignant glioma patients with HLA-A * 24/A * 02 allele. Cytotherapy *14*, 733–742.
18. Pollack, I.F., Jakacki, R.I., Butterfield, L.H., Hamilton, R.L., Panigrahy, A., Potter, D.M., Connelly, A.K., Dibridge, S.A., Whiteside, T.L., and Okada, H. (2014). Antigen-specific immune responses and clinical outcome after vaccination with glioma-associated antigen peptides and polyinosinic-polycytidylic acid stabilized by lysine and carboxymethylcellulose in children with newly diagnosed malignant brainstem and nonbrainstem gliomas. J. Clin. Oncol. *32*, 2050–2058.
19. Yin, Y., Boesteanu, A.C., Binder, Z.A., Xu, C., Reid, R.A., Rodriguez, J.L., Cook, D.R., Thokala, R., Blouch, K., McGettigan-Croce, B., et al. (2018). Checkpoint blockade reverses anergy in IL-13Ra2 humanized scFv-based CAR T cells to treat murine and canine gliomas. Mol. Ther. Oncolytics *11*, 20–38.
20. Brown, C.E., Alizadeh, D., Starr, R., Weng, L., Wagner, J.R., Naranjo, A., Ostberg, J.R., Blanchard, M.S., Kilpatrick, J., Simpson, J., et al. (2016). Regression of glioblastoma after chimeric antigen receptor T-cell therapy. N. Engl. J. Med. *375*, 2561–2569.
21. Brown, C.E., Badie, B., Barish, M.E., Weng, L., Ostberg, J.R., Chang, W.C., Naranjo, A., Starr, R., Wagner, J., Wright, C., et al. (2015). Bioactivity and safety of IL13Rα2-redirected chimeric antigen receptor CD8+ T cells in patients with recurrent glioblastoma. Clin. Cancer Res. *21*, 4062–4072.
22. Pituch, K.C., Miska, J., Krenciute, G., Panek, W.K., Li, G., Rodriguez-Cruz, T., Wu, M., Han, Y., Lesniak, M.S., Gottschalk, S., et al. (2018). Adoptive transfer of IL13Ra2-specific chimeric antigen receptor T cells creates a pro-inflammatory environment in glioblastoma. Mol. Ther. *26*, 986–995.
23. Janssen. (2021). RYBREVANT™ (Amivantamab-vmjw) Receives FDA Approval as the First Targeted Treatment for Patients with Non-small Cell Lung Cancer with EGFR Exon 20 Insertion Mutations.
24. Bortoletto, N., Scotet, E., Myamoto, Y., D'Oro, U., and Lanzavecchia, A. (2002). Optimizing anti-CD3 affinity for effective T celltargeting against tumor cells. Eur. J. Immunol. *32*, 3102–3107.
25. Haber, L., Olson, K., Kelly, M.P., Crawford, A., DiLillo, D.J., Tavaré, R., Ullman, E., Mao, S., Canova, L., Sineshchekova, O., et al. (2021). Generation of T-cell-redirecting bispecific antibodies with differentiated profiles of cytokine release and biodistribution by CD3 affinity tuning. Sci. Rep. 14397.
26. Poussin, M., Sereno, A., Wu, X., Huang, F., Manro, J., Cao, S., Carpenito, C., Glasebrook, A., Powell, D.J., and Demarest, S. (2021). Dichotomous impact of affinity on the function of T cell engaging bispecific antibodies. J. Immunother. Cancer *9*, e002444.
27. Staflin, K., Zuch de Zafra, C.L., Schutt, L.K., Clark, V., Zhong, F., Hristopoulos, M., Clark, R., Li, J., Mathieu, M., Chen, X., et al. (2020). Target arm affinities determine preclinical efficacy and safety of anti-HER2/CD3 bispecific antibody. JCI Insight *5*, 133757.
28. Perales-Puchalt, A., Duperret, E.K., Muthumani, K., and Weiner, D.B. (2019). Simplifying checkpoint inhibitor delivery through in vivo generation of synthetic DNA-encoded monoclonal antibodies (DMAbs). Oncotarget *10*, 13–16.
29. Duperret, E.K., Trautz, A., Stoltz, R., Patel, A., Wise, M.C., Perales-Puchalt, A., Smith, T., Broderick, K.E., Masteller, E., Kim, J.J., et al. (2018). Synthetic DNA-encoded monoclonal antibody delivery of anti-CTLA-4 antibodies induces tumor shrinkage in vivo. Cancer Res. *78*, 6363–6370.
30. Patel, A., Park, D.H., Davis, C.W., Smith, T.R.F., Leung, A., Tierney, K., Bryan, A., Davidson, E., Yu, X., Racine, T., et al. (2018). In vivo delivery of synthetic human DNA-encoded monoclonal antibodies protect against ebolavirus infection in a mouse model. Cell Rep. *25*, 1982–1993.e4.
31. Pituch, K.C., Zannikoua, M., Ilut, L., Xiao, T., Chastkofsky, M., Sukhanova, M., Bertolino, N., Procissi, D., Amidei, C., Horbinski, C.M., et al. (2021). Neural stem cells secreting bispecific T cell engager to induce selective antiglioma activity. PNAS, 118.

32. Sternjak, A., Lee, F., Thomas, O., Balazs, M., Wahl, J., Lorenczewski, G., Ullrich, I., Muenz, M., Rattel, B., Bailis, J.M., et al. (2021). Preclinical assessment of AMG 596, a bispecific T-cell engager (BiTE) immunotherapy targeting the tumor-specific antigen EGFRvIII. Mol. Cancer Ther. *20*, 925–933.

33. Bonifant, C.L., Szoor, A., Torres, D., Joseph, N., Velasquez, M.P., Iwahori, K., Gaikwad, A., Nguyen, P., Arber, C., Song, X.T., et al. (2016). CD123-Engager T cells as a novel immunotherapeutic for acute myeloid leukemia. Mol. Ther. *24*, 1615–1626.

34. Wunderlich, M., Brooks, R.A., Panchal, R., Rhyasen, G.W., Danet-Desnoyers, G., and Mulloy, J.C. (2014). OKT3 prevents xenogeneic GVHD and allows reliable xenograft initiation from unfractionated human hematopoietic tissues. Blood *123*, 134–144.

35. Guil-Luna, S., Sedlik, C., and Piaggio, E. (2021). Humanized mouse models to evaluate cancer immunotherapeutics. Annu. Rev. Cancer Biol. *5*, 119–136.

36. Yaguchi, T., Kobayashi, A., Inozume, T., Morii, K., Nagumo, H., Nishio, H., Iwata, T., Ka, Y., Katano, I., Ito, R., et al. (2018). Human PBMC-transferred murine MHC class I/II-deficient NOG mice enable long-term evaluation of human immune responses. Cell. Mol. Immunol. *15*, 953–962.

37. Stastny, M.J., Brown, C.E., Ruel, C., and Jensen, M.C. (2007). Medulloblastomas expressing IL13Rα2 are targets for IL13-zetakine+ cytolytic T cells. J. Pediatr. Hematol. Oncol. *29*, 669–677.

38. Kawakami, M., Kawakami, K., Kasperbauer, J.L., Hinkley, L.L., Tsukuda, M., Strome, S.E., and Puri, R.K. (2003). Interleukin-13 receptor α2 chain in human head and neck cancer serves as a unique diagnostic marker. Clin. Cancer Res. *9*, 6381–6388.

39. Kioi, M., Kawakami, M., Shimamura, T., Husain, S.R., and Puri, R.K. (2006). Interleukin-13 receptor alpha2 chain: a potential biomarker and molecular target for ovarian cancer therapy. Cancer *107*, 1407–1418.

40. Beard, R.E., Abate-Daga, D., Rosati, S.F., Zheng, Z., Wunderlich, J.R., Rosenberg, S.A., and Morgan, R.A. (2013). Gene expression profiling using nanostring digital RNA counting to identify potential target antigens for melanoma immunotherapy. Clin. Cancer Res. *19*, 4941–4950.

41. Shibasaki, N., Yamasaki, T., Kanno, T., Arakaki, R., Sakamoto, H., Utsunomiya, N., Inoue, T., Tsuruyama, T., Nakamura, E., Ogawa, O., et al. (2015). Role of IL13RA2 in sunitinib resistance in clear cell renal cell carcinoma. Plos One *10*, e0130980.